Supporting Information

Integrating NiFe Bimetal Sites into Conjugated Microporous Polymer for Boosting Photocatalytic Selective Aromatic Alcohols Oxidation

Shien Guo,[1] Zhen Yu,[1] Chao Xu,[2] Zhipeng Wang,[1] Wei Tao,[1] Qiaoya Tang,[1] Zhenghui Liu,[3] and Yuting Xiao[2]**

[1] Institute of Advanced Materials (IAM), College of Chemistry and Chemical Engineering, Jiangxi Normal University, Nanchang 330022, People's Republic of China.

[2] Key Laboratory of Jiangxi Province for Persistent Pollutants Control and Resources Recycle, Nanchang Hangkong University, Nanchang 330063, People's Republic of China.

[3] Department of Chemistry, Taizhou University, Taizhou 318000, Zhejiang, People's Republic of China

Table of Contents

Materials

5,5'-dibromo-2,2'-bipyridyl, tetrakis(4-ethynylphenyl)porphyrin, diisopropylamine, tetrakis(triphenylphosphine)palladium, copper(I) iodide, cobalt(II) acetate, iron(III) chloride, toluene, N,N-Dimethylformamide, 1,4-dioxane, dichloromethane, benzyl alcohol, $CDCl_3$, and methanol were purchased from Macklin, all the chemicals were used directly without further purification.

Characterizations

Nitrogen adsorption/desorption isotherm was measured at 77 K on a Micromeritics ASAP 2010 analyzer, the sample was activated under vacuum at 150 ℃ overnight prior to measure. The powder X-ray diffraction (XRD) was recorded on a D8 Advance diffractometer with Cu Kα radiation (λ=0.15418 nm) in the 2θ range from 5~80º. The morphology and microstructure were observed by scanning electron microscope (SEM, Hitachi S-4800) and transmission electron microscopy (TEM, Tecnai G2 F20). The UV-vis diffuse reflectance spectra (DRS) were measured on a Varian Cary 5000 UV-vis spectrophotometer with pure white $BaSO_4$ as the reference. X-ray photoelectron spectroscopy (XPS) measurements were analyzed using an ESCA-Lab-200i-XL spectrometer (PHI, USA) with monochromatic Al Kα radiation (1486.6 eV). Fourier transformation infrared spectra (FT-IR) were recorded on a Nicolet 6700 (Thermo Fisher, USA). Samples were dried and compressed to a plate with KBr for measurement. Steady-state photoluminescence (PL) spectra were collected by a FluoroMax-4 spectrofluorometer (Horiba Scientific). The time-resolved fluorescence decay spectra were measured by FLS980 spectrometer (Edinburgh Instruments, UK). The nickel and ferric contents were measured by the inductively coupled plasma-atomic emission spectrometer (ICP-AES) using the iCAP 7400 spectrometer (Thermo Fisher Scientific, USA).

Photoelectrochemical measurements

All electrochemical and photoelectrochemical measurements were conducted using a

three-electrode system on an electrochemical workstation (CHI-660C, Shanghai Chenhua). The working electrode consisted of a piece of FTO glass with a prepared photocatalyst coating. The counter electrode was a platinum plate, while the reference electrode was Ag/AgCl. The electrolyte used was a Na_2SO_4 solution (0.2 M). For the photoelectrochemical measurement, the same light source as the photocatalysis experiment was used. Mott-Schottky diagrams were obtained at frequencies of 1000 and 1300 Hz. The transient photocurrent response was recorded intermittently under visible light irradiation, while electrochemical impedance spectroscopy was obtained under dark conditions.

Computational methods

All the DFT calculations were conducted based on the Vienna Ab-inito Simulation Package (VASP).[1] The exchange-correlation effects were described by the Perdew-Burke-Ernzerhof (PBE) functional within the generalized gradient approximation (GGA) method.[2] The core-valence interactions were accounted by the projected augmented wave (PAW) method.[3] The energy cutoff for plane wave expansions was set to 400 eV, and the 2×2×1 Monkhorst-Pack grid k-points were selected to sample the Brillouin zone integration. The structural optimization was completed for energy and force convergence set at 1.0×10-4 eV and 0.05 eV $Å^{-1}$, respectively. Grimme's DFT-D3 methodology[4] was used to describe the dispersion interactions.

The adsorption energies (E_{ads}) are calculated by

$$E_{ads} = E_{*O2} – E_{O2} – E_{sub}$$

where E_{O2} and E_{*O2} represent the energies before and after the adsorption of O_2 on the substrate, respectively. E_{sub} is the energy of clean surface.

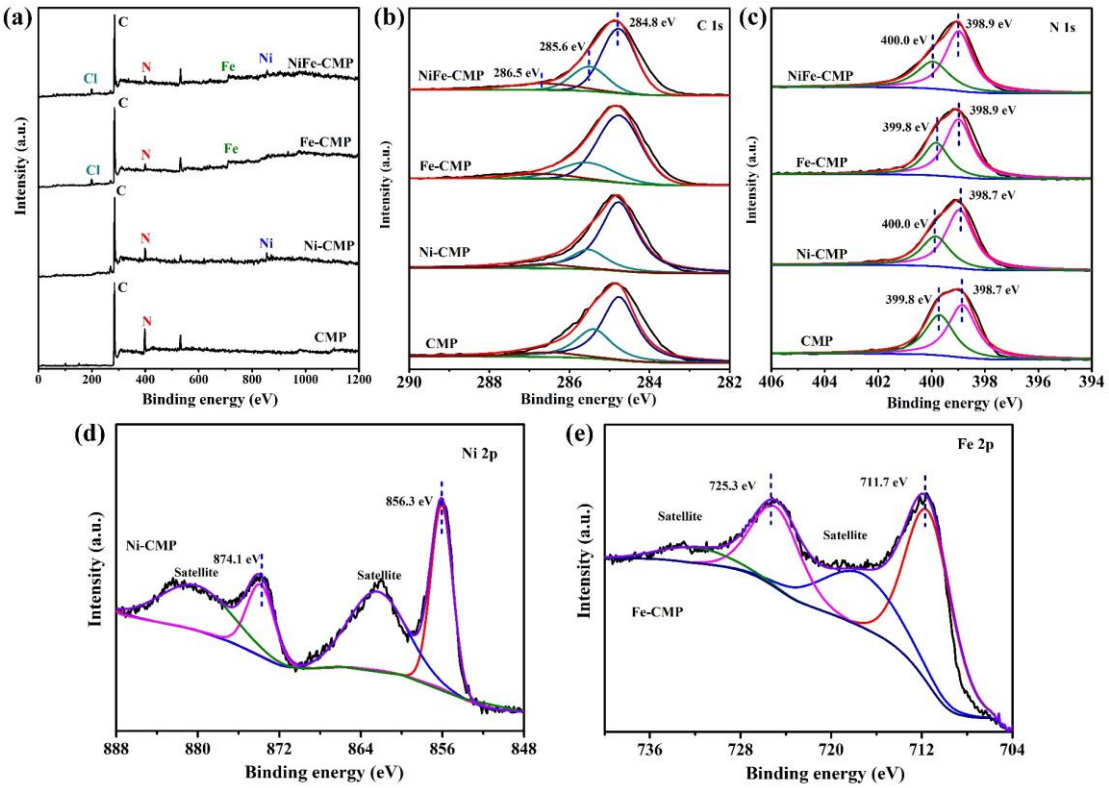

Fig. S1. (a) XPS survey, (b) C 1s and (c) N 1s spectra of CMP, Ni-CMP, Fe-CMP and NiFe-CMP. (d) Ni 2p spectrum of Ni-CMP, (e) Fe 2p spectrum of Fe-CMP.

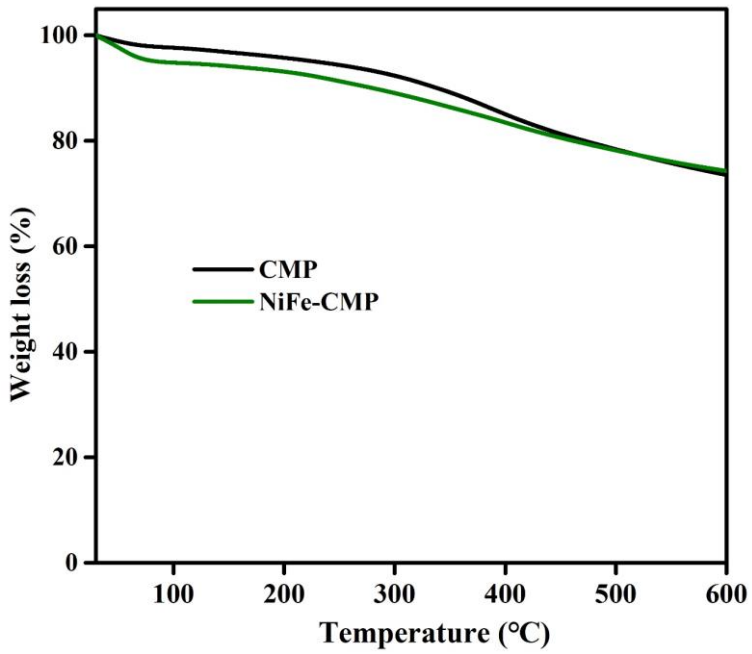

Fig. S2. Thermogravimetric analysis (TGA) curve of CMP and NiFe-CMP under N_2 atmosphere

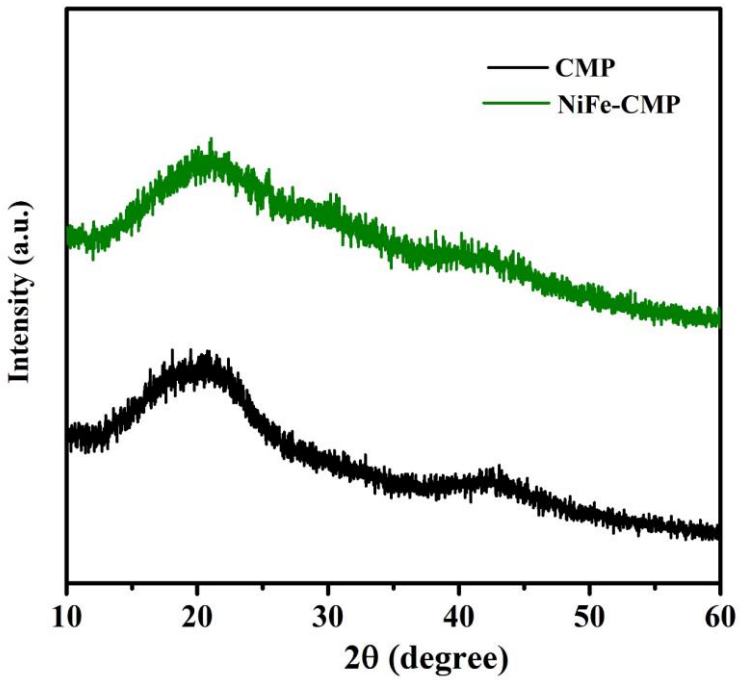

Fig. S3. XRD patterns of CMP and NiFe-CMP.

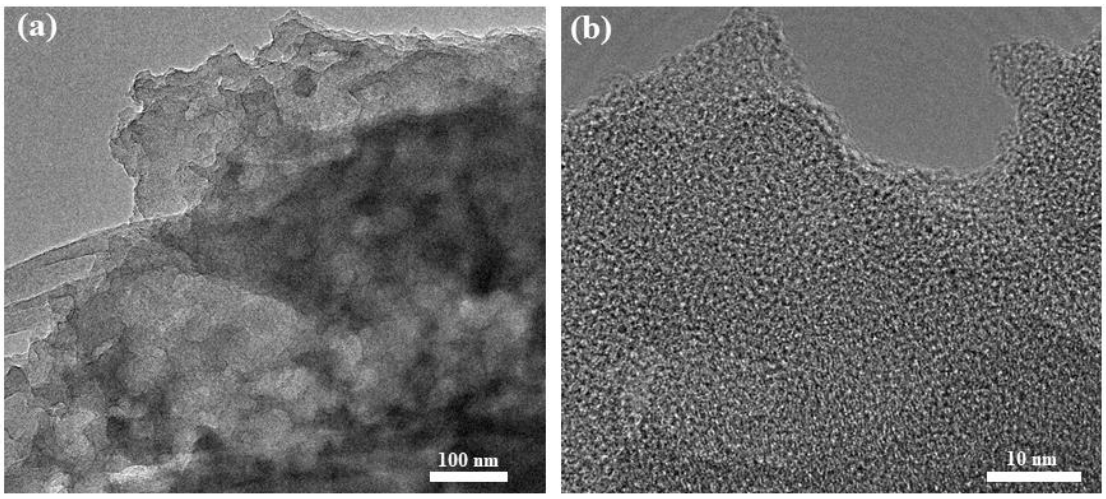

Fig. S4. (a) TEM and (b) high-resolution TEM images of CMP.

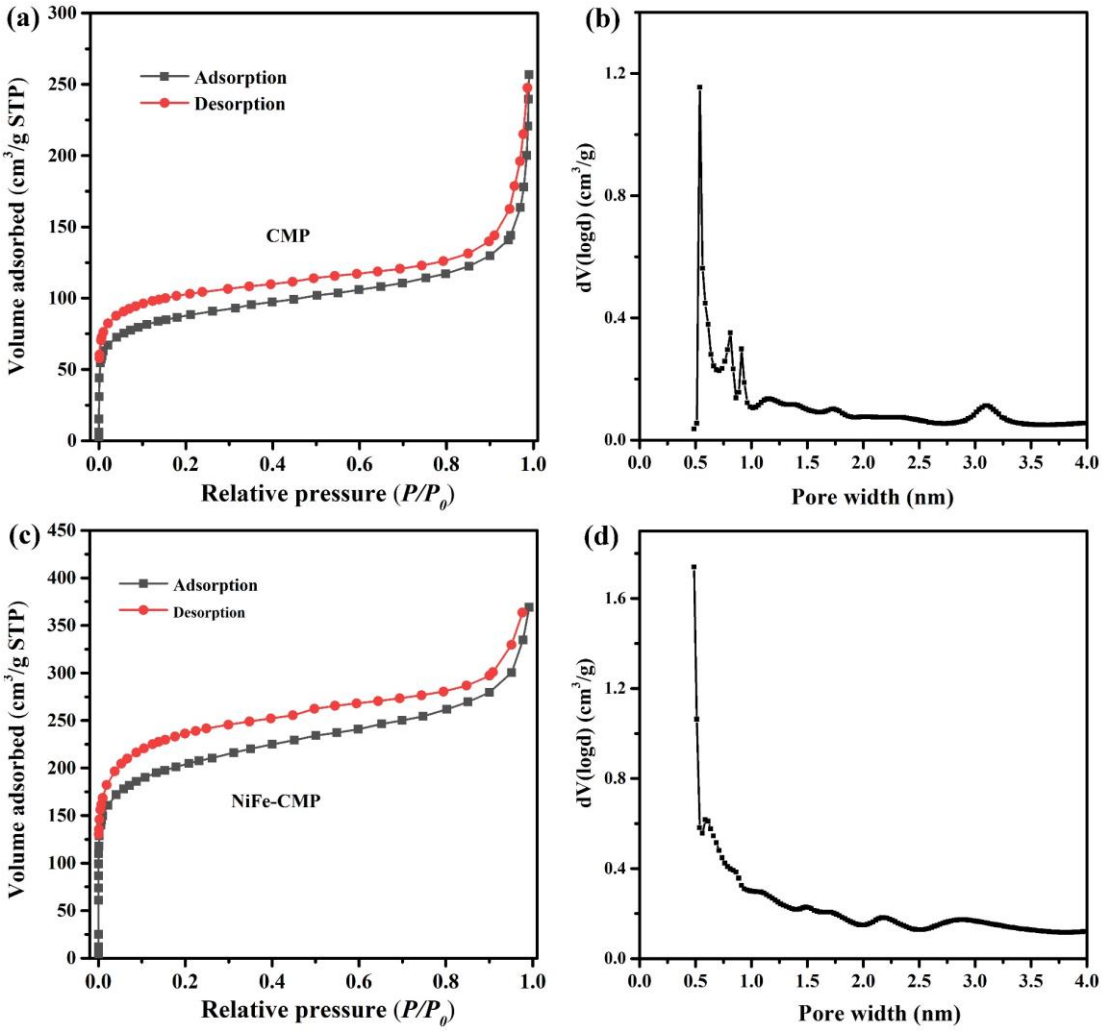

Fig. S5. Nitrogen adsorption-desorption isotherms and corresponding pore size distributions of (a-b) CMP and (c-d) NiFe-CMP.

Table S1. Influence of the solvent in photooxidation of benzyl alcohol.

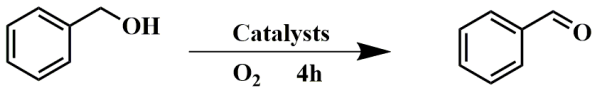

Entry	Catalysts (mg)	Solvent	Conversion (%)	Selectivity (%)
1	10	CH_3CN	68.4	99
2	10	1,4-dioxane	87.5	99
3	10	DMF	46.7	99
4	10	DMAC	55.1	99
5	10	DMSO	12.4	99
6	10	NMP	71.8	99

Table S2. Influence of the catalyst amount and reaction time on photooxidation of benzyl alcohol.

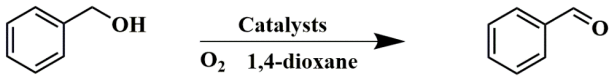

Entry	Visible Light	Catalysts (mg)	Time (h)	Conversion (%)	Selectivity (%)
1	on	10	1	44.3	99
2	on	10	2	65.9	99
3	on	10	3	83.4	99
4	on	10	4	96.2	99
5	on	10	5	98.1	99
6	on	2	4	62.2	99
7	on	5	4	82.4	99
8	on	20	4	94.8	99

Table S3. The photocatalytic selective oxidation of benzyl alcohol over different photocatalysts reported in the literature.

Sample	Catalyst (mg)	Substrate (mmol)	Light source	Reaction time	Conv. (%)	Sel. (%)	Reference
BiOCl	30	0.05	Xe lamp (350-780 nm)	5 h	99	98	[5]
$Bi_4Ti_3O_{12}$	10	0.1	Xe (> 360nm)	5 h	35.5	99.8	[6]
$CsPbBr_3/W_{18}O_{49}$	10	0.1	Xe lamp	8 h	72	99	[7]
$W_{18}O_{49}$/HUCNS	20	0.1	Xe lamp	1 h	39.8	99.8	[8]
ZnTi-LDH	20	0.1	Xe lamp	4 h	61	77	[9]
TiO_2/Ti_3C_2	30	0.02	Xe lamp	5 h	97	98	[10]
ZFO/U6N	20	0.2	Xe lamp AM 1.5G	5 h	68	99	[11]
MIL-125-NH_2	100	1	Xe lamp (350-780 nm)	4 h	13.6	99	[12]
UiO-66-NH_2					17.1	99	
NiFe-CMP	**10**	**1**	**Xe lamp (400-780 nm)**	**4 h**	**96.2**	**99**	**This work**

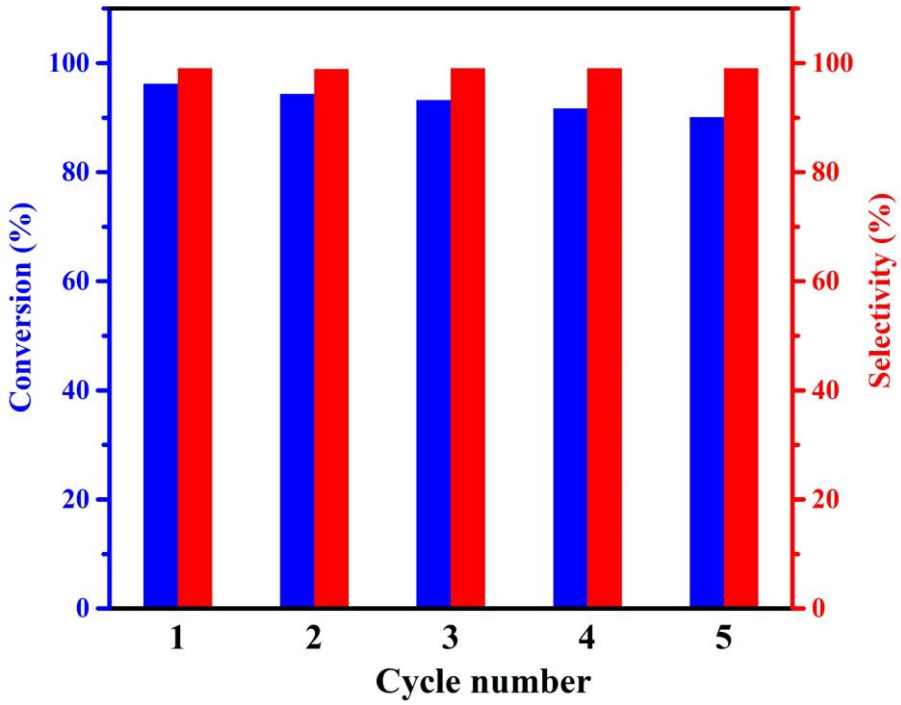

Fig. S6. Recyclability study on NiFe-CMP for the photooxidation of benzyl alcohol under visible light.

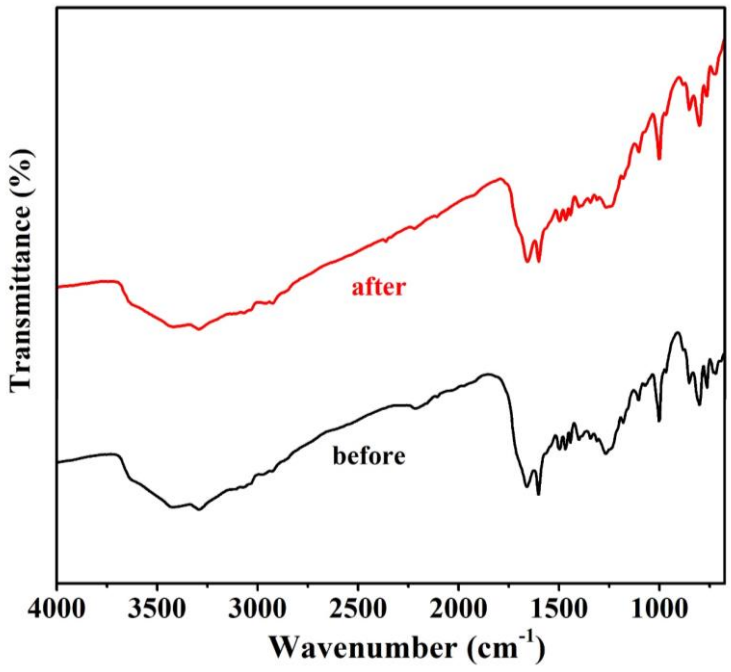

Fig. S7. FT-IR spectra of NiFe-CMP before and after cycling test.

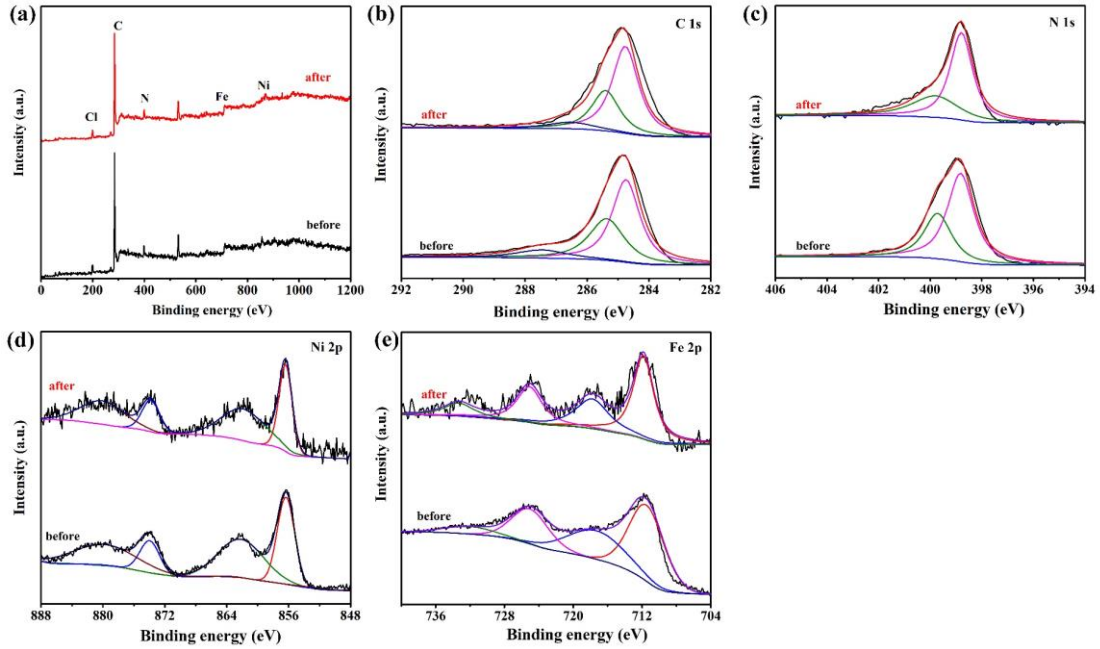

Fig. S8. XPS spectra of NiFe-CMP before and after the cycling tests. Full spectra (a), High-resolution (b) C 1s, (c) N 1s (d) Ni 2p and (e) Fe 2p.

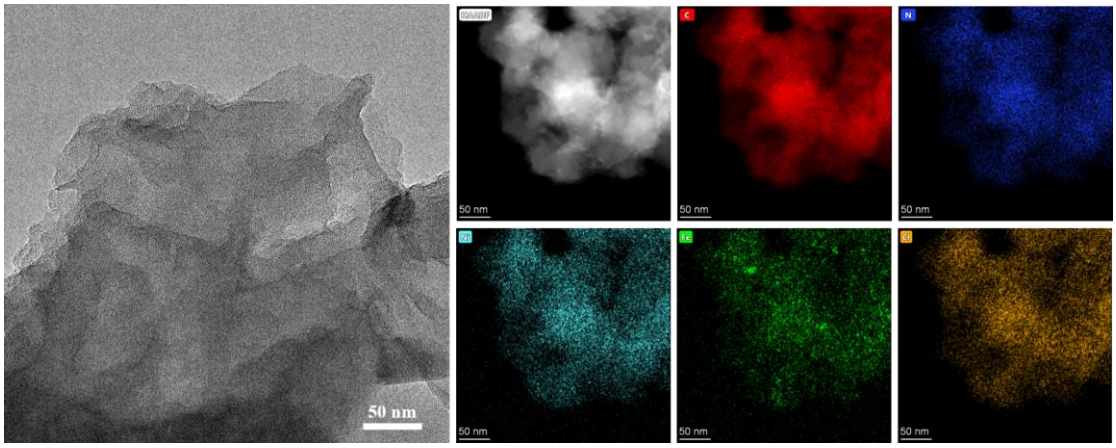

Fig. S9. TEM images and corresponding EDX elemental mapping images of NiFe-CMP after photocatalytic reaction.

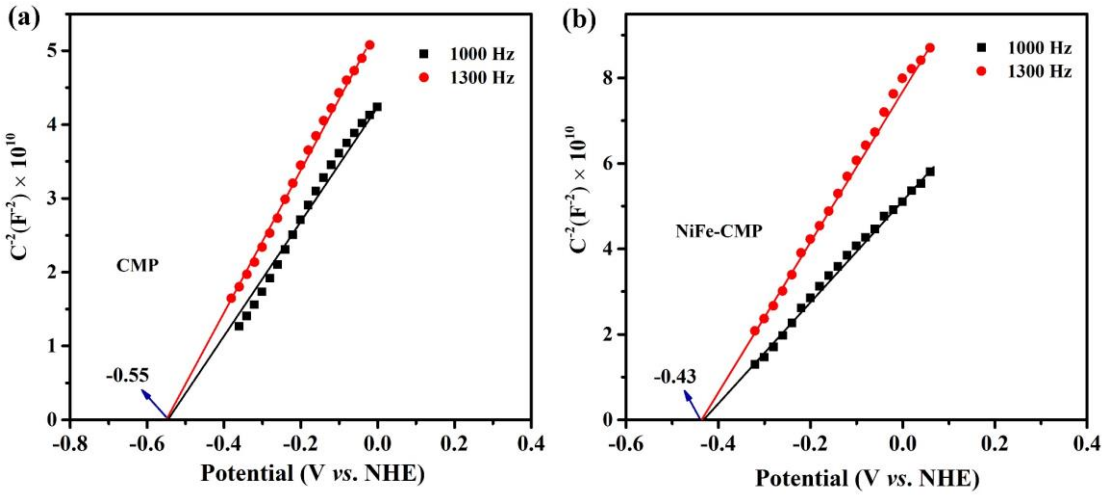

Fig. S10. Mott-Schottky plots of (a) CMP and (b) NiFe-CMP samples collected at various frequencies.

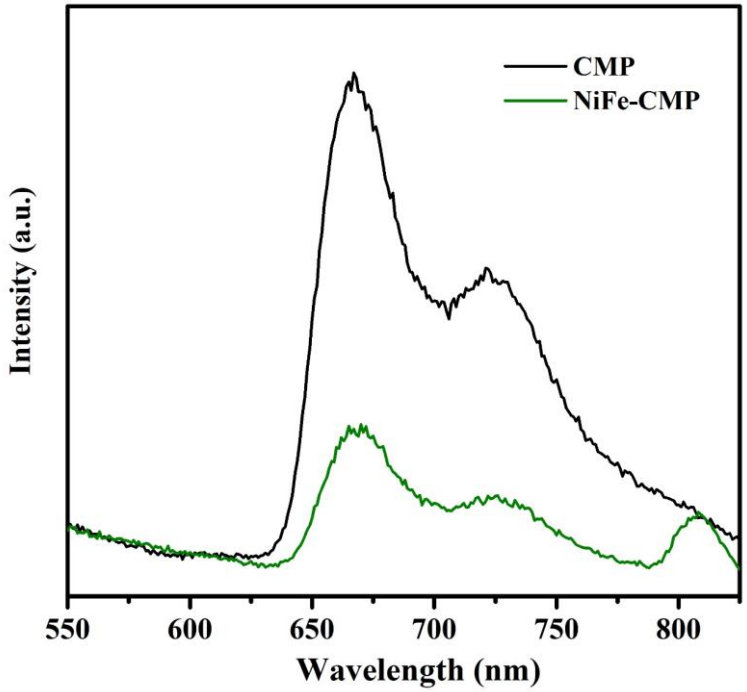

Fig. S11. Steady state PL spectra of CMP and NiFe-CMP at excitation wavelength of 375 nm.

Table S4. Fitted parameters from time-resolved PL spectra of CMP and NiFe-CMP.

Photocatalysts	τ_1	Rel.%	τ_2	Rel.%	τ
CMP	1.85	35.46	6.92	64.54	6.27
NiFe-CMP	1.21	44.68	5.16	55.32	4.53

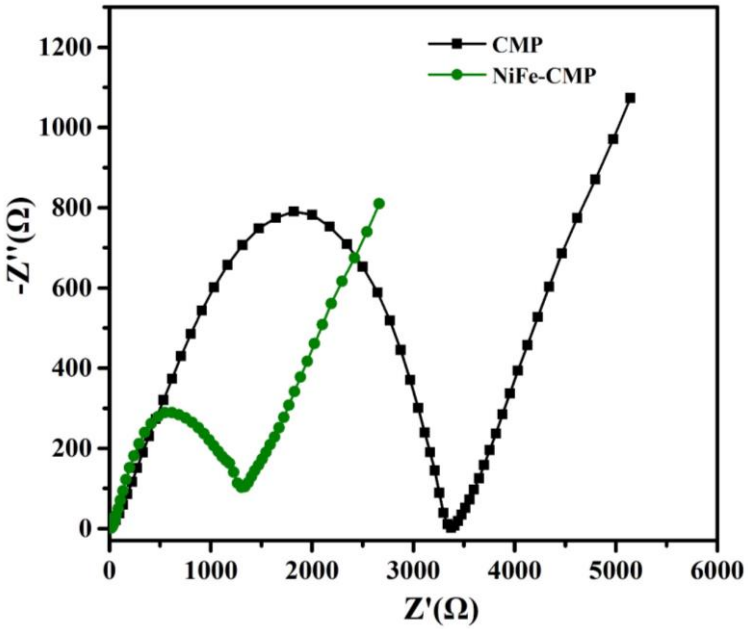

Fig. S12. Nyquist plots of electrochemical impedance spectra for CMP and NiFe-CMP.

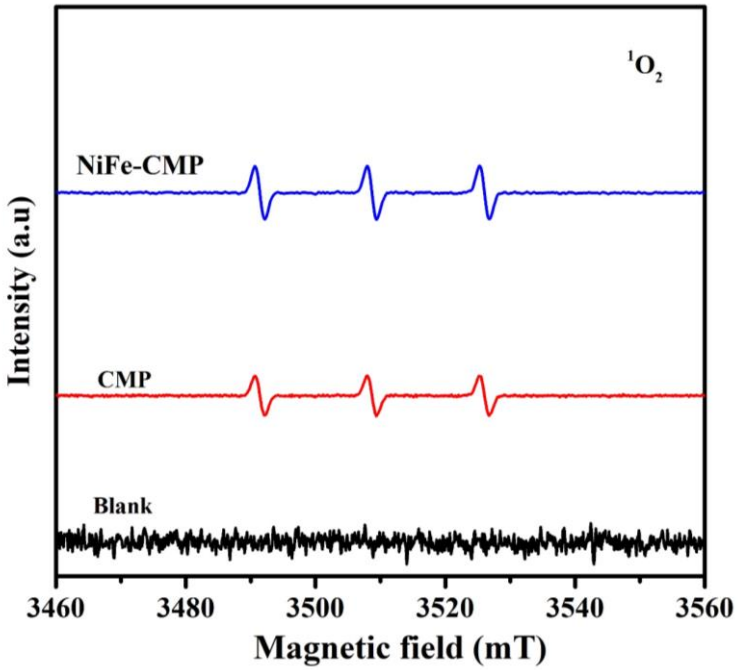

Fig. S13. Spin-trapping EPR spectra of TEMPO-$^1O_2$ for CMP and NiFe-CMP.

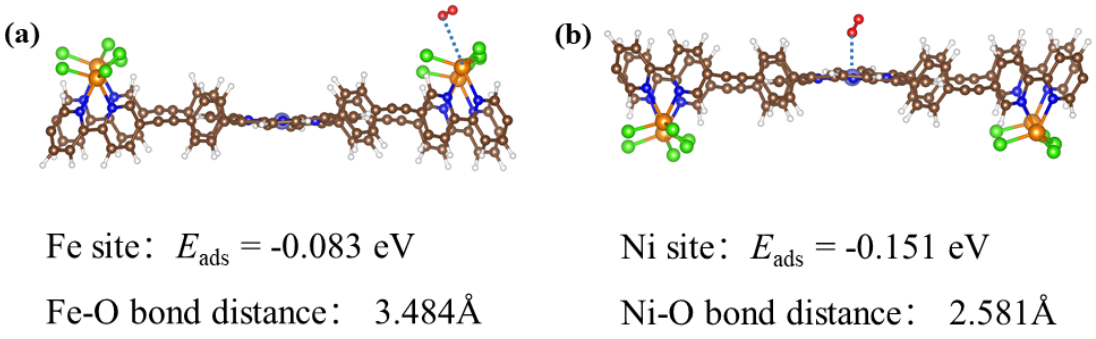

Fig. S14. DFT-derived O_2 binding structures of Fe and Ni sites for NiFe-CMP.

Reference:

[1] Kresse, G.; Hafner, J. Ab initio molecular-dynamics simulation of the liquid-metal–amorphous-semiconductor transition in germanium. *Phys. Rev. B* **1994**, 49, 14251.

[2] Perdew, J. P.; Burke, K.; Ernzerhof, M. Generalized gradient approximation made simple. *Phys. Rev. Lett.* **1996**, 77, 3865.

[3] Blöchl, P. E. Projector augmented-wave method. *Phys. Rev. B* **1994**, 50, 17953.

[4] Grimme, S.; Antony, J.; Ehrlich, S.; Krieg, H. A consistent and accurate ab initio parametrization of density functional dispersion correction (DFT-D) for the 94 elements H-Pu. *J. Chem. Phys.* **2010**, 132.

[5] Li, W.; Mao, Y.; Liu, Z.; Zhang, J.; Luo, J.; Zhang, L.; Qiao, Z.-A. Chelated Ion-Exchange Strategy toward BiOCl Mesoporous Single-Crystalline Nanosheets for Boosting Photocatalytic Selective Aromatic Alcohols Oxidation. *Adv. Mater.* **2023**, 35, 2300396.

[6] Shen, M.; Shi, Y.; Wang, Z.; Wu, T.; Hu, L.; Wu, L. Enhanced photocatalytic benzyl alcohol oxidation over $Bi_4Ti_3O_{12}$ ultrathin nanosheets. *J. Colloid Interf. Sci.* **2022**, 608, 2529-2538.

[7] Cheng, R.; Steele, J. A.; Roeffaers, M. B.; Hofkens, J.;Debroye, E. Dual-channel charge carrier transfer in $CsPbX_3$ perovskite/$W_{18}O_{49}$ composites for selective photocatalytic benzyl alcohol oxidation. *ACS Appl. Energy Mater.* **2021**, 4, 3460-3468.

[8] Xiao, C.; Zhang, L.; Hao, H.; Wang, W. High selective oxidation of benzyl alcohol to benzylaldehyde and benzoic acid with surface oxygen vacancies on $W_{18}O_{49}$/holey ultrathin g-C_3N_4 nanosheets. *ACS Sustain. Chem. Eng.* **2019**, 7, 7268-7276.

[9] Zou, J.; Wang, Z.; Guo, W.; Guo, B.; Yu, Y.; Wu, L. Photocatalytic selective oxidation of benzyl alcohol over ZnTi-LDH: The effect of surface OH groups. *Appl. Catal. B.* **2020**, 260, 118185.

[10] Bao, X.; Li, H.; Wang, Z.; Tong, F.; Liu, M.; Zheng, Z.; Wang, P.; Cheng, H.; Liu, Y.; Dai, Y. TiO_2/Ti_3C_2 as an efficient photocatalyst for selective oxidation of benzyl alcohol to benzaldehyde. *Appl. Catal. B.* **2021**, 286, 119885.

[11] Liu, J.; Sun, X.; Jiang, B.; Liu, M.; Li, Q.; Xiao, X.; Wang, H.; Zheng, M.; Guo, S.; Wu, J.; Zhang, Y.; Shi, K.; Zhou, W. UiO-66-NH_2 Octahedral Nanocrystals Decorated with $ZnFe_2O_4$ Nanoparticles for Photocatalytic Alcohol Oxidation. *ACS Appl. Nano Mater.* **2022**, 5, 2231-2240.

[12] Qiu, J.; Zhang, X.; Xie, K.; Zhang, X.-F.; Feng, Y.; Jia, M.; Yao, J. Noble metal nanoparticle-functionalized Zr-metal organic frameworks with excellent photocatalytic performance. *J. Colloid Interf. Sci.* **2019**, 538, 569-577.